Cell Reports
Article

The Histone-H3K4-Specific Demethylase KDM5B Binds to Its Substrate and Product through Distinct PHD Fingers

Brianna J. Klein,[1,11] Lianhua Piao,[2,11] Yuanxin Xi,[3] Hector Rincon-Arano,[4] Scott B. Rothbart,[5] Danni Peng,[2] Hong Wen,[2] Connie Larson,[6] Xi Zhang,[2] Xia Zheng,[3] Michael A. Cortazar,[7] Pedro V. Peña,[1] Anthony Mangan,[7] David L. Bentley,[7,8] Brian D. Strahl,[5] Mark Groudine,[4,9] Wei Li,[3] Xiaobing Shi,[2,6,10,*] and Tatiana G. Kutateladze[1,7,*]

[1]Department of Pharmacology, University of Colorado School of Medicine, Aurora, CO 80045, USA
[2]Department of Biochemistry and Molecular Biology, The University of Texas MD Anderson Cancer Center, Houston, TX 77030, USA
[3]Dan L. Duncan Cancer Center, Department of Molecular and Cellular Biology, Baylor College of Medicine, Houston, TX 77030, USA
[4]Basic Science Division, Fred Hutchinson Cancer Research Center, Seattle, WA 98109, USA
[5]Department of Biochemistry and Biophysics and the Lineberger Comprehensive Cancer Center, University of North Carolina School of Medicine, Chapel Hill, NC 27599, USA
[6]Genes and Development Graduate Program, The University of Texas Graduate School of Biomedical Sciences, Houston, TX 77030, USA
[7]Molecular Biology Program, University of Colorado School of Medicine, Aurora, CO 80045, USA
[8]Department of Biochemistry and Molecular Genetics, University of Colorado School of Medicine, Aurora, CO 80045, USA
[9]Department of Radiation Oncology, University Washington School of Medicine, Seattle, WA 98109, USA
[10]Center for Cancer Epigenetics and Center for Stem Cell and Developmental Biology, The University of Texas MD Anderson Cancer Center, Houston, TX 77030, USA
[11]These authors contributed equally to this work
*Correspondence: xbshi@mdanderson.org (X.S.), tatiana.kutateladze@ucdenver.edu (T.G.K.)
http://dx.doi.org/10.1016/j.celrep.2013.12.021

SUMMARY

The histone lysine demethylase KDM5B regulates gene transcription and cell differentiation and is implicated in carcinogenesis. It contains multiple conserved chromatin-associated domains, including three PHD fingers of unknown function. Here, we show that the first and third, but not the second, PHD fingers of KDM5B possess histone binding activities. The PHD1 finger is highly specific for unmodified histone H3 (H3K4me0), whereas the PHD3 finger shows preference for the trimethylated histone mark H3K4me3. RNA-seq analysis indicates that KDM5B functions as a transcriptional repressor for genes involved in inflammatory responses, cell proliferation, adhesion, and migration. Biochemical analysis reveals that KDM5B associates with components of the nucleosome remodeling and deacetylase (NuRD) complex and may cooperate with the histone deacetylase 1 (HDAC1) in gene repression. KDM5B is downregulated in triple-negative breast cancer relative to estrogen-receptor-positive breast cancer. Overexpression of KDM5B in the MDA-MB 231 breast cancer cells suppresses cell migration and invasion, and the PHD1-H3K4me0 interaction is essential for inhibiting migration. These findings highlight tumor-suppressive functions of KDM5B in triple-negative breast cancer cells and suggest a multivalent mechanism for KDM5B-mediated transcriptional regulation.

INTRODUCTION

The histone lysine demethylase KDM5B (also known as PLU-1 and JARID1B) regulates gene expression and is implicated in cancer development and proliferation (Klose et al., 2006). KDM5B belongs to the KDM5/JARID1 family, which catalyzes the removal of methyl groups from tri-, di-, and monomethylated lysine 4 of histone H3 (H3K4me3/2/1), and also includes KDM5A/RBP2, KDM5C/SMCX, and KDM5D/SMCY in mammals (Christensen et al., 2007; Iwase et al., 2007; Klose et al., 2007; Yamane et al., 2007). Both fly and yeast have a single ortholog of KDM5: the *Drosophila* Little imaginal disks (Lid) and *S. cerevisiae* Jhd2p/Yjr119Cp, respectively (Eissenberg et al., 2007; Lee et al., 2007; Liang et al., 2007; Secombe et al., 2007; Seward et al., 2007). The KDM5 proteins have a highly conserved domain architecture. They contain a catalytic JmjN/JmjC domain, a DNA binding ARID/Bright domain, a C5HC2 zinc finger, and two or three PHD fingers, with the exception of yeast KDM5, which consists of only the catalytic module and one PHD finger.

The expression of the *KDM5B* gene is restricted in normal adult tissues, except for testes and ovaries, but it is often upregulated in human malignancies, including breast, prostate, bladder, lung, and cervical cancers, and leukemias (Hayami et al., 2010; Roesch et al., 2010; Xiang et al., 2007). KDM5B interacts with transcription factors PAX9, FOXG1, and FOXC2 (reviewed in Cloos et al., 2008) and associates with nuclear receptors such as estrogen receptor alpha (ERα), androgen

receptor, and progesterone receptor to repress or promote activation of target genes (Catchpole et al., 2011; Krishnakumar and Kraus, 2010; Vicent et al., 2013; Xiang et al., 2007). Microarray analyses have revealed that KDM5B represses genes of antiproliferative and cell-cycle regulators, including the tumor suppressor BRCA1, HOX5A, and metallothioneins in the mammary epithelial cancer cell line MCF7, while positively regulating E2F1 and E2F2 in A549 and SW789 cells (Hayami et al., 2010; Scibetta et al., 2007; Yamane et al., 2007). Knockdown of KDM5B decreases the growth of MCF7 cells both in vitro and in vivo, suggesting that KDM5B is required for the proliferation in this type of cancer (Catchpole et al., 2011; Li et al., 2011; Yamane et al., 2007).

Recent studies have implicated KDM5B in the continuous growth of xenografted melanoma cells and metastatic progression (Roesch et al., 2010), and overexpression of KDM5B in immortalized normal breast cancer MCF10A cells was found to enhance cell invasion (Yoshida et al., 2011). However, in addition to functioning as an oncoprotein, KDM5B has been shown to possess tumor-suppressive activities. KDM5B associates with the retinoblastoma (Rb) tumor suppressor, and KDM5B knockdown phenocopies loss of Rb in Rb-dependent senescence models (Chicas et al., 2012; Nijwening et al., 2011; Roesch et al., 2005). Consistent with its tumor-suppression function, overexpression of KDM5B in the triple-negative breast cancer cell line MDA-MB 231 inhibits cell migration and invasion potentials (Li et al., 2011). Thus, growing evidence suggests that KDM5B can act as an oncoprotein or a tumor suppressor in a cell-type-dependent manner. However, the molecular mechanism by which KDM5B contributes to gene regulation and exerts opposite functions in carcinogenesis remains unclear.

In this work, we show that KDM5B functions as a broad transcriptional repressor for genes involved in inflammatory response, cell proliferation, cell adhesion, and migration in MDA-MB 231 triple-negative breast cancer cells. Mass spectrometry, immunoprecipitation (IP), and genomic analyses demonstrate that KDM5B associates with components of the NuRD complex and may cooperate with the HDAC1 deacetylase and the CHD4 ATPase in repression. We found that of the three PHD fingers present in KDM5B, two (PHD1 and PHD3) bind to histone tails. Whereas PHD1 is highly specific for H3K4me0, PHD3 is more promiscuous and recognizes H3K4me3 as well as lower methylation states of H3K4. KDM5B inhibits the migration and invasion abilities of MDA-MB 231 breast cancer cells, and binding of the PHD1 finger to H3K4me0 is required to suppress cell migration. Together, our data highlight tumor-suppressive functions of KDM5B in triple-negative breast cancer cells and suggest a multivalent mechanism underlying KDM5B-dependent repression.

RESULTS AND DISCUSSION

KDM5B Is Downregulated in ER$^-$ Breast Cancer Cells

Breast cancer is a heterogeneous disease. Molecular profiling has identified several distinct subtypes of breast cancer, which correlate with hormone response, patient prognosis, and response to therapy (Morris and Carey, 2007). KDM5B has been shown to play a significant role in breast cancer progression and metastatic capacity (Catchpole et al., 2011; Li et al., 2011; Yamane et al., 2007); however, it remains unclear whether KDM5B has the same expression and tumorigenic activities in different subtypes of tumors. To clarify this, we examined the expression levels of KDM5B in 12 different breast cancer cell lines (Figure 1A). Cell nuclear extracts were isolated and probed with anti-KDM5B. In comparison to immortalized "normal" breast cancer cells (76NF2V and MCF-10A), KDM5B was overexpressed in ER$^+$ cells, including MCF7, T47D, MDA-MB 361, and UACC 812 (Figure 1A). Surprisingly, we found that the expression level of KDM5B was significantly lower in ER$^-$ cells, including HER2$^+$ SKBR3 and AU565 cells, and the triple-negative MDA-MB 231, MDA-MB 436, and MDA-MB 468 cells. The triple-negative subtype of breast cancer is particularly associated with worse survival prognosis in comparison with ER$^+$ breast cancers. To determine the general expression level of KDM5B in the triple-negative subtype, we analyzed *KDM5B* gene expression in breast cancer patients in the Curtis breast tumor data set available in Oncomine. We observed lower expression levels of *KDM5B* in the triple-negative breast cancer patients compared with patients with the ER$^+$/PR$^+$ subtype (Figure S1; Table S1).

The differential expression levels of KDM5B imply distinct roles of this protein in ER$^+$ and ER$^-$ cancer subtypes. Although the function of KDM5B in ER$^+$ MCF7 cells was previously characterized (Catchpole et al., 2011; Li et al., 2011; Scibetta et al., 2007; Yamane et al., 2007), little is known about KDM5B activities in more aggressive ER$^-$ subtypes. To assess the role of KDM5B in triple-negative breast cancer, we used two small hairpin RNAs (shRNAs) that reduced the KDM5B protein level to different degrees in MDA-MB 231 cells. As shown in Figure 1B, full knockdown of KDM5B led to increased H3K4me3 levels, which is consistent with the H3K4-specific demethylase activity of KDM5B. It also indicates that the orthologous KDM5 demethylases do not substitute for KDM5B, which has also been observed in ER$^+$ MCF7 cells (Catchpole et al., 2011; Yamane et al., 2007).

KDM5B Is Required for Repression of a Set of Genes Involved in Immune Response and Cell Proliferation in MDA-MB 231 Cells

To identify KDM5B-regulated genes in MDA-MB 231 cells on a genome-wide scale, we performed RNA sequencing (RNA-seq) gene-expression analysis in cells treated with a KDM5B-target shRNA or a control nontargeting shRNA in duplicates. We identified 423 genes that were upregulated and 333 genes that were downregulated in KDM5B knockdown MDA-MB 231 cells (Figure 1C). These results imply that KDM5B correlates with both gene activation and repression. Gene Ontology (GO) analysis revealed that KDM5B represses genes involved in immune response and cell proliferation, as well as regulation of angiogenesis, cell adhesion, and migration, whereas downregulated genes in KDM5B knockdown cells did not cluster (Figure 1C; Table S2). The expression of the KDM5B-dependent genes was further validated by quantitative real-time PCR (Figure 1D). A substantial increase in gene expression was seen in both KDM5B-knockdown cells, and the extent of upregulation inversely correlated with the extent of KDM5B knockdown,

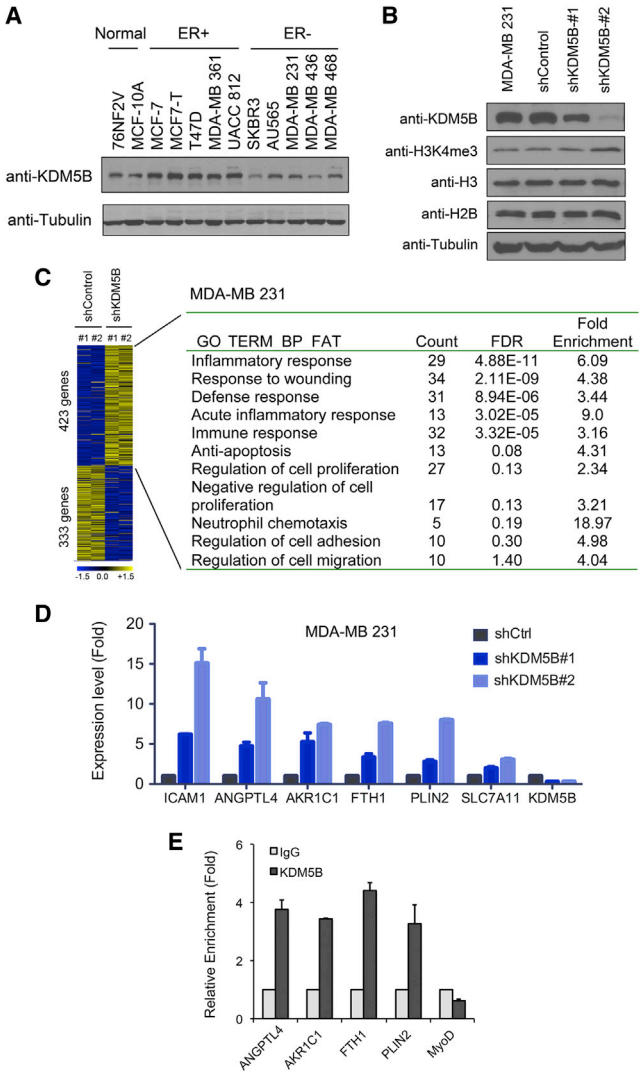

Figure 1. KDM5B Is a Broad Transcriptional Repressor

(A) KDM5B is overexpressed in ER-positive (ER^+) but downregulated in ER-negative (ER^-) breast cancer cells. Western blot analysis of KDM5B protein levels across a panel of breast cancer cells is shown.

(B) Knockdown of KDM5B leads to increased global H3K4me3 levels. Western blot analysis of KDM5B and H3K4me3 levels in KDM5B knockdown and control cells.

(C) KDM5B represses the expression of genes involved in immune response, proliferation, and migration. A heatmap of up- and downregulated genes in MDA-MB 231 cells treated with KDM5B-specific shRNA versus control shRNA is shown. GO analysis of upregulated genes is shown on the right. Downregulated genes are not enriched in any specific GO term with false discovery rate (FDR) < 5 (see Table S2).

(D) Quantitative real-time PCR analysis of the expression of KDM5B-regulated genes in control and KDM5B knockdown MDA-MB 231 cells. Error bars represent SEM.

(E) KDM5B ChIP analysis on the promoters of the indicated genes in MDA-MB 231 cells stably expressing Flag-KDM5B. Immunoglobulin G (IgG) is shown as a negative control. Error bars represent SEM.

See also Figure S1 and Tables S1 and S2.

suggesting that the observed differences are caused by the elimination of KDM5B. Furthermore, chromatin IP (ChIP) assays in KDM5B-overexpressing cells demonstrated that KDM5B binds to the promoters of these genes, substantiating that these genes are likely KDM5B direct targets (Figure 1E). Together, these results suggest that KDM5B represses a set of target genes in MDA-MB 231 cells.

KDM5B Associates with the Deacetylase NuRD Complex

The mechanism underlying transcriptional repression by KDM5B is not well understood, and the question of whether it relies on the demethylase activity per se or encompasses other epigenetic processes remains open. To examine whether KDM5B is capable of associating with other nuclear proteins, we immunoprecipitated KDM5B from human embryonic kidney 293 (HEK293) cells stably expressing Flag-tagged KDM5B, followed by SDS-PAGE and silver staining (Figure 2A). Mass spectrometry and western blot analyses of the IP purification showed that KDM5B coprecipitated with two catalytic subunits of the NuRD complex (reviewed in Allen et al., 2013). One subunit is a chromodomain helicase DNA binding protein 4 (CHD4) ATPase, which hydrolyses ATP necessary for DNA sliding and repositioning of nucleosomes. The second catalytic subunit is histone deacetylase 1 (HDAC1), which deacetylates acetylated lysine residues of histones. Furthermore, two noncatalytic subunits of NuRD, metastasis-associated 2 (MTA2) and retinoblastoma binding protein 4 (RBBP4), were also identified. A direct interaction between KDM5B and HDAC4 was previously reported (Barrett et al., 2007); therefore, we tested whether KDM5B is able to associate with HDAC1. CoIP experiments in cells transfected with Flag-HDAC1 demonstrated that HDAC1 indeed interacts with endogenous KDM5B (Figure 2B). These data suggest the intriguing possibility of a cooperative action of the three catalytic components, coupling lysine demethylation, lysine deacetylation, and ATPase-mediated chromatin remodeling, all of which are important for transcriptional repression (Figure 2C).

KDM5B Colocalizes with HDAC1 and CHD4 at Chromatin

To confirm that KDM5B, HDAC1, and CHD4 colocalize in vivo, we performed an analysis of ChIP-seq data sets generated by the ENCODE consortium in K562 cells. KDM5B is recruited to ~140,000 genomic regions, and ~50% (76,268 out of 140,000) of these regions overlap with the regions occupied by HDAC1 (Figure 2D). Furthermore, 99% of the CHD4-bound regions overlap with the KDM5B-HDAC1-bound regions, which represents ~17% (12,811 out of 76,268) of KDM5B-HDAC1 associations. Together, these results suggest a strong co-occupancy of KDM5B with the NuRD complex on the chromatin.

The genome-wide analysis revealed that ~50% of the KDM5B-HDAC1 binding sites overlap with tri-, di-, or monomethylated H3K4 (H3K4me3/2/1), which are substrates for the KDM5B enzymatic activity (Figures 2E and S2). Notably, ~95% of the KDM5B-HDAC1-CHD4-bound regions correlate with chromatin enriched in H3K4me3, and these regions comprise ~50% of the KDM5B-HDAC1-H3K4me3 overlapping regions (Figures 2F and S2). Active, weak, or poised promoters and enhancers were particularly occupied by

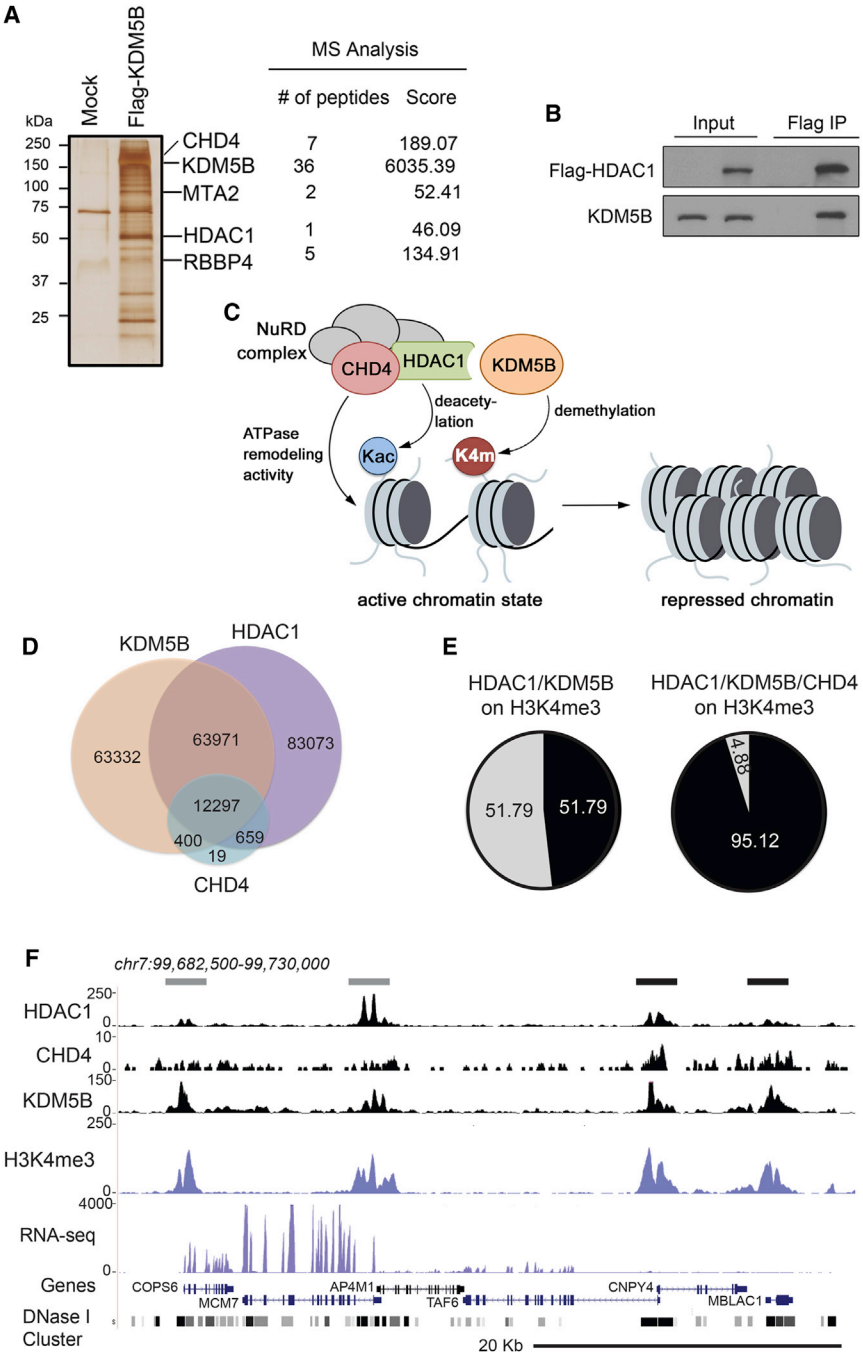

Figure 2. KDM5B Associates with Components of the NuRD Complex

(A) Mass-spectrometric analysis of the KDM5B protein complex. Silver staining of the IP-purified complex and the number of peptides and scores of KDM5B-associated proteins are shown.

(B) CoIP of KDM5B with HDAC1.

(C) A model for the cooperative action of KDM5B and the NuRD complex.

(D) Venn diagram showing overlap of the KDM5B-, HDAC1-, and CHD4-bound genomic regions.

(E) Overlaps of the H3K4me3-, KDM5B-HDAC1-, and KDM5B-HDAC1-CHD4-bound regions are shown in black.

(F) KDM5, HDAC1, and CHD4 chromatin profiles over a 50 Kb region of human chromosome 7. Peaks are indicated with a black line and a gray line over the profiles for KDM5B-HDAC1-CHD4 and KDM5B-HDAC1, respectively. ChIP-seq data for H3K4me3 and RNA-seq in K562 cells are shown. The two lower tracks correspond to the coding regions containing exons and introns, as well as DNase I-accessible regions.

See also Figure S2.

KDM5B-HDAC1-CHD4. These results imply that KDM5B colocalizes with the NuRD components at the sites that contain its substrate (H3K4me3), the removal of which by KDM5B would yield transcriptionally inactive chromatin.

PHD1 and PHD3 Fingers of KDM5B, but Not PHD2, Have Histone Binding Activity

KDM5B contains three PHD fingers, the biological roles of which remain unclear (Figure 3A). Because PHD fingers from other proteins have recently been shown to possess histone binding activity, we generated individual KDM5B PHD finger constructs (PHD1, PHD2, and PHD3) and tested these proteins in pull-down assays and histone peptide microarrays. Glutathione S-transferase (GST)-fusion PHD1, PHD2, and PHD3 fingers were incubated first with biotinylated histone peptides containing single methylation marks and then with streptavidin Sepharose beads. The histone peptide-bound proteins were detected by western blotting. As shown in Figure 3B, the KDM5B PHD1 finger recognizes the N terminus of histone H3, either unmodified or methylated at Lys9. The second finger (PHD2) was incapable of histone binding, whereas the third finger (PHD3) showed a preference for H3K4me3. This high specificity was confirmed by using an extended peptide microarray. The PHD1 finger bound to histone H3 (H3K4me0) regardless of posttranslational modifications (PTMs) present on Lys9, Lys14, or Lys18, whereas PHD3 was specific for methylated H3K4 (Figure S3).

To examine the effect of the PTMs commonly found in the first six residues of histone H3 on binding of the KDM5B PHD fingers, we hybridized these proteins to a PTM library microarray (Figures 3C and 3D). The GST-tagged PHD fingers were screened against an extensive library of multiply modified histone peptides (Table S3). In agreement with the pull-down data, the KDM5B PHD1 finger associated with unmodified histone H3 tail; however,

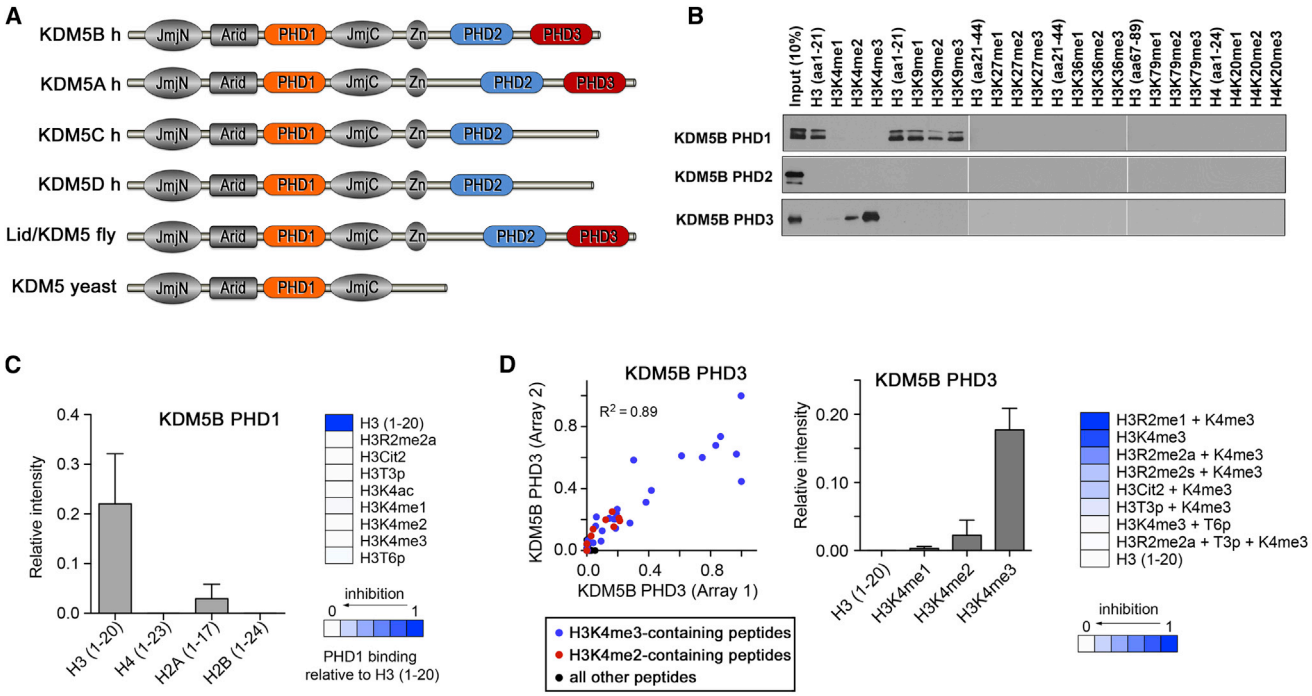

Figure 3. The KDM5B PHD1 and PHD3 Fingers, but Not PHD2, Show Histone Binding Activity

(A) Schematic representation of the KDM5 family of proteins.

(B) Western blot analysis of GST-KDM5B PHD fingers bound to the indicated biotinylated peptides.

(C and D) GST-KDM5B PHD1 and PHD3 were analyzed on a PTM library microarray. Relative average signal intensities are shown in graphs. Error bars represent SEM from pooled averages of two independent array experiments. A scatterplot of two arrays probed with GST-KDM5B PHD3 is also shown. Blue and red dots indicate H3K4me3-containing and H3K4me2-containing peptides, respectively. The correlation coefficient was calculated by linear regression analysis using GraphPad Prism v5. A list of the PTM-containing peptides used in the assays and a complete analysis are provided in Tables S3 and S4, respectively. See also Figure S3.

PTMs on the first six residues of H3 blocked this interaction. In particular, dimethylation or citrullination of Arg2, phosphorylation of Thr3, methylation of Lys4, and phosphorylation of Thr6 were not tolerated. On the other hand, binding of the PHD3 finger to H3K4me3 was affected to a lesser extent. PTMs of Arg2 were permissible, whereas phosphorylation of Thr3 reduced this interaction and phosphorylation of Thr6 further inhibited it.

Mechanism of H3K4me0 Recognition by PHD1

To determine the molecular basis for the interaction between KDM5B PHD1 and unmodified histone H3, we purified ^{15}N-labeled protein and carried out ^{1}H,^{15}N heteronuclear single quantum coherence (HSQC) titration experiments (Figure 4). Addition of the H3K4me0 peptide (aa 1–12 of H3) induced large chemical-shift changes in the PHD1 finger, indicating direct binding (Figure 4A). A number of peaks disappeared at a protein-to-peptide ratio of 1:1 and many changed their positions, revealing slow-to-intermediate exchange regime on the nuclear magnetic resonance (NMR) timescale, indicative of a strong interaction. The precise binding affinity of the KDM5B PHD1 finger for H3K4me0 was found to be 1.5 μM, as measured by fluorescence spectroscopy (Figure 4E).

To identify residues in the histone binding site of the PHD1 finger, we produced a ^{13}C/^{15}N-labeled KDM5B PHD1 finger. We assigned backbone and side-chain ^{1}H, ^{13}C, and ^{15}N chemical shifts using a set of 3D triple-resonance experiments and analyzed perturbations in the ^{1}H, ^{15}N HSQC spectra of the protein upon binding to H3K4me0. Plotting chemical-shift changes for each backbone amide allowed us to identify the residues of KDM5B PHD1 that were directly or indirectly involved in the interaction (Figure 4B). The most perturbed residues were clustered in the middle region of the PHD1 finger sequence, encompassing residues E321–C330, and a shorter region around W351 was perturbed to a lesser degree. To obtain mechanistic details of the interaction, we used the assigned ^{13}Cα, ^{13}Cβ, ^{1}Hα, ^{15}N, and ^{1}HN chemical shifts and a chemical-shift Rosetta (CS-Rosetta) protocol (Shen et al., 2008) to generate a model of the apo state. The resulting model showed a typical PHD/RING finger fold and was superimposed with the structure of the CHD4 PHD2 finger with an rmsd of 2 Å. Mapping the KDM5B residues with significantly perturbed amide resonances onto the model diagram revealed that these residues are located in or around the first β strand of the PHD1 finger (Figure 4C). This binding site is in good agreement with the binding sites seen in previously determined structures of PHD fingers bound to H3K4me0 (reviewed in Musselman and Kutateladze, 2011).

To assess the inhibition effect of Lys4 methylation, we characterized the interaction of the KDM5B PHD1 finger with H3K4me1,

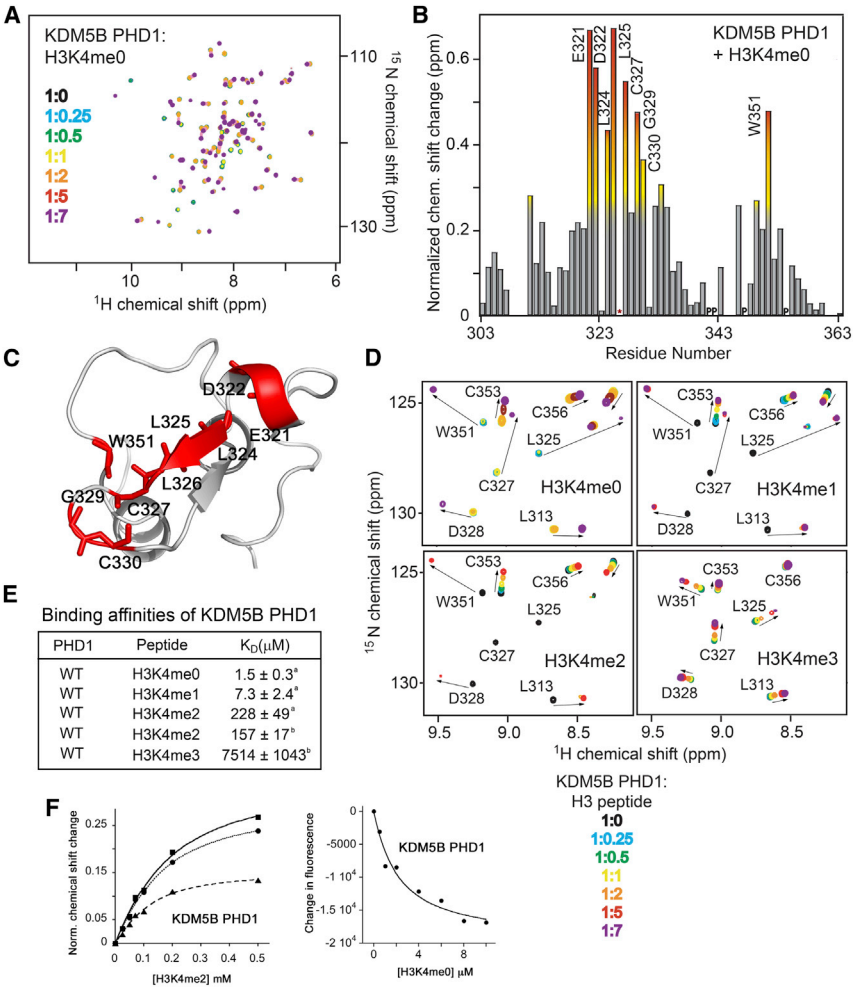

PHD1	Peptide	K_D(µM)
WT	H3K4me0	1.5 ± 0.3[a]
WT	H3K4me1	7.3 ± 2.4[a]
WT	H3K4me2	228 ± 49[a]
WT	H3K4me2	157 ± 17[b]
WT	H3K4me3	7514 ± 1043[b]

Figure 4. The PHD1 Finger of KDM5B Is Specific for H3K4me0

(A) Superimposed ^{1}H,^{15}N HSQC spectra of KDM5B PHD1 collected upon titration of H3K4me0 peptide. Spectra are color-coded according to the protein:peptide molar ratio.

(B) Normalized chemical-shift changes observed in the PHD1 finger upon binding to H3K4me0 as a function of residue. Differences greater than the average plus 1 SD, the average plus 0.5 SD, and the average are shown in red, orange, and yellow, respectively. An asterisk indicates disappearance of a signal.

(C) Model of the PHD1 finger fold generated using assigned ^{13}Cα, ^{13}Cβ, ^{1}Hα, ^{15}N, and ^{1}HN chemical shifts and a CS-Rosetta protocol. The most perturbed residues of the PHD1 finger in (B) are colored red and labeled.

(D) Superimposed ^{1}H,^{15}N HSQC spectra of KDM5B PHD1 collected upon titration with H3K4me0, H3K4me1, H3K4me2, and H3K4me0 peptides (residues 1–12 of H3).

(E) Binding affinities of WT KDM5B PHD1 for the indicated histone peptides measured by tryptophan fluorescence ([a]) or NMR ([b]).

(F) Representative binding curves used to determine K_D values by fluorescence and NMR.

H3K4me2, and H3K4me3 peptides by NMR and fluorescence spectroscopy (Figures 4D and 4E). We found that the PHD1 finger binds to H3K4me1 and H3K4me2 peptides 5- and 100-fold more weakly than it binds to H3K4me0 (Figure 3C). Trimethylated H3K4me3 peptide caused very small changes in the protein NMR spectra, indicating an almost negligible association in the millimolar range of affinities.

The H3K4me0 Binding Mode Is Conserved

The elongated histone binding site of KDM5B PHD1 and high sequence similarity suggest that the binding mode of this protein is similar to that of the AIRE, BHC80, CHD4, and TRIM24 PHD fingers, and this was supported by mutational analysis (Figures 4C and 5A). ^{1}H,^{15}N HSQC and pull-down experiments showed that substitution of L326, a conserved hydrophobic residue preceding the third zinc-coordinating Cys, to a tryptophan abolished interaction of KDM5B PHD1 with H3K4me0 (Figures 5B–5D). Likewise, replacement of the corresponding hallmark Cys or Met residues in other H3K4me0-specific PHD fingers with a bulky tryptophan completely disrupts this binding (Lan et al., 2007; Musselman et al., 2009). Another distinguishable feature of the H3K4me0 recognition is the presence of extensive acidic patches on the surface of a PHD finger that are involved in electrostatic and hydrogen-bonding contacts with unmodified lysine and arginine residues of H3. Although the KDM5B PHD1 sequence N-terminal to the first zinc-coordinating Cys is less acidic than the sequences of other H3K4me0 binding PHD fingers, KDM5B contains more acidic residues in the loop connecting the zinc-coordinating second and third Cys residues, as well as following the fourth zinc-coordinating Cys (Figure 5A). Whereas replacement of some surface acidic residues with an alanine resulted in insoluble proteins, soluble D320A and D328A mutants showed a decrease in binding to H3K4me0, corroborating the importance of electrostatic contacts with the highly basic H3K4me0 tail (Figures 5B–5D).

Although the sequences of human KDM5B PHD1, human KDM5D PHD1, and a single PHD finger of yeast KDM5 are very similar, KDM5D and the yeast ortholog bound to H3K4me0 much more weakly in comparison to KDM5B (Figure 5A; Figures 5E and 5F, left). The respective equilibrium dissociation constants (K_Ds) were measured by means of ^{1}H,^{15}N HSQC titrations and found to be 3.5 mM and 117 µM, respectively. Such a weak association was not enhanced by methylation of H3K9, as was found for the CHD4 PHD fingers (Figure 5E, right), and the reduction of the surface negative charge further diminished it (Figure 5F, right). Notably, the key L326 residue in the KDM5B sequence is replaced by a phenylalanine in KDM5D (Figure 5A). Much like a tryptophan in the L326W mutant of KDM5B, the bulky phenylalanine may cause steric hindrance, impeding this interaction. Another critical residue, an invariable

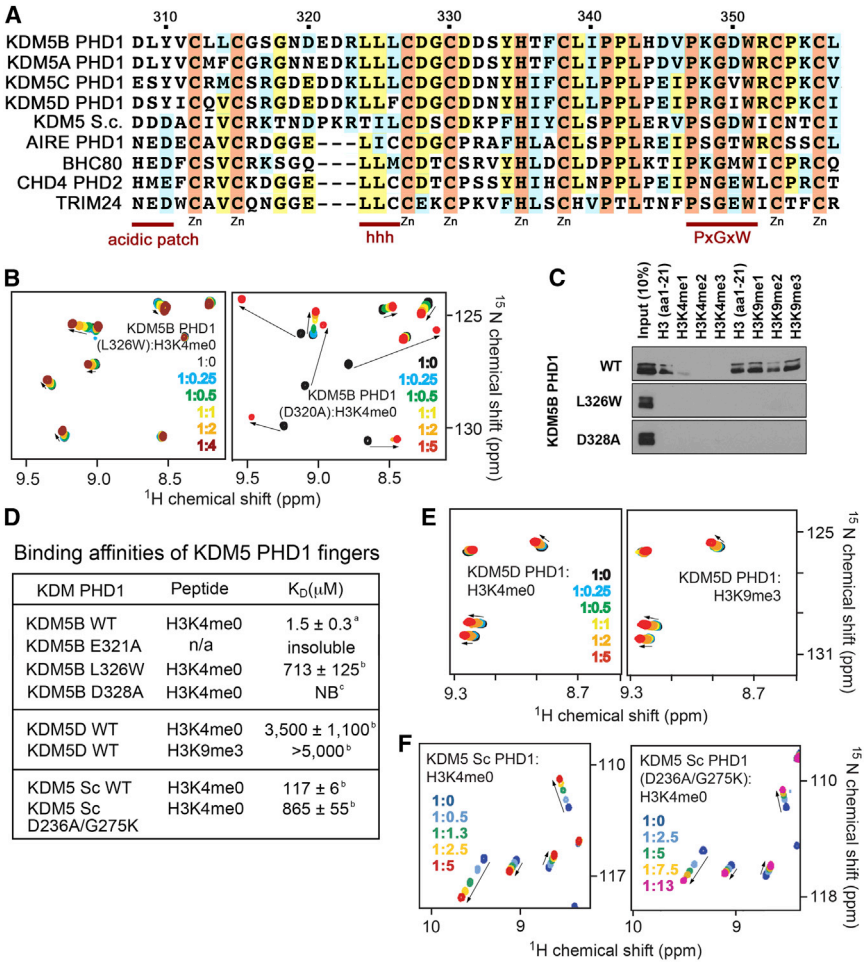

KDM PHD1	Peptide	K_D(μM)
KDM5B WT	H3K4me0	1.5 ± 0.3[a]
KDM5B E321A	n/a	insoluble
KDM5B L326W	H3K4me0	713 ± 125[b]
KDM5B D328A	H3K4me0	NB[c]
KDM5D WT	H3K4me0	3,500 ± 1,100[b]
KDM5D WT	H3K9me3	>5,000[b]
KDM5 Sc WT	H3K4me0	117 ± 6[b]
KDM5 Sc D236A/G275K	H3K4me0	865 ± 55[b]

Figure 5. The Molecular Mechanism of the KDM5B PHD1-H3K4me0 Interaction

(A) Alignment of the PHD finger sequences; absolutely, moderately, and weakly conserved residues are colored pink, yellow, and blue, respectively. Regions that are important for the interaction with H3K4me0 are indicated by red bars. Each tenth residue of KDM5B is labeled.

(B) Overlays of $^{1}H,^{15}N$ HSQC spectra of the PHD1 L326W and D320A mutants collected upon titration of the H3K4me0 peptide.

(C) Western blot analysis of GST-KDM5B PHD1, WT, and mutants bound to the biotinylated peptides.

(D) Binding affinities of human KDM5B, human KDM5D, and yeast KDM5 PHD1 fingers for the indicated histone peptides measured by tryptophan fluorescence ([a]) or NMR ([b]). NB, no binding by western blot ([c]).

(E and F) Overlays of $^{1}H,^{15}N$ HSQC spectra of the PHD1 fingers of KDM5D and yeast KDM5 collected upon titration of the indicated peptides. Spectra are color-coded according to the protein:peptide molar ratio.

leucine (L324 in KDM5B), is substituted by a threonine in yeast KDM5, most likely accounting for the decrease in binding (Figure 5A).

The PHD3 Finger Prefers H3K4me3 but Also Binds H3K4me0

The amino acid sequence of the PHD3 finger of KDM5B has 70% identical residues compared with the sequence of the PHD3 finger of KDM5A, including the two tryptophan residues that were previously shown to be required for binding to H3K4me3 (Wang et al., 2009; Figures 6 and S4). Accordingly, mutation of the W1502 and W1512 residues in KDM5B PHD3 disrupted interaction with H3K4me3, whereas replacement of acidic D1506 with an arginine reduced it (Figures 6C–6E). These results imply that the mechanism of H3K4me3 recognition by the PHD3 finger of KDM5A is conserved in KDM5B, with W1502 and W1512 of the KDM5B PHD3 finger most likely being involved in caging the trimethylammonium group of H3K4me3 and D1506, contributing to restraining the guanidino group of Arg2 of the histone peptide. Surprisingly, we found that the KDM5B PHD3 finger shows only a slight preference for the trimethylated state of H3K4. We compared interactions with histone H3K4me3/2/1/0 peptides using NMR and fluorescence spectroscopy (Figures 6B and 6D). An almost identical pattern of chemical-shift changes induced by H3K4me3, H3K4me2, H3K4me1, and H3K4me0 in the $^{1}H,^{15}N$ HSQC spectra of PHD3 suggested that these peptides occupy the same binding pocket (Figure 6B). The slow-exchange regime on the NMR timescale for the methylated peptides revealed an equally robust interaction. Even interaction with the unmodified peptide was in the slow-to-intermediate exchange, which is indicative of strong binding. In agreement, the binding affinities of the KDM5B PHD3 finger for all four peptides were in the range of 0.5–4 μM, as measured by fluorescence spectroscopy (Figure 6D). Together, these data demonstrate that the KDM5B PHD3 finger binds strongly to either methylated or unmodified histone H3K4, but it prefers the trimethylated species.

PHD1-H3K4me0 Interaction Is Important for Suppression of MDA-MB 231 Cell Migration

Our GO analysis of MDA-MB 231 cells suggested that in triple-negative breast cancer cells, KDM5B represses genes involved in the regulation of cell adhesion and migration, the two processes that are imperative for cancer metastasis. We therefore sought to examine the role of KDM5B and its PHD fingers in cell migration and invasion. Consistent with the GO analysis, knockdown of KDM5B in MDA-MB 231 cells increased the cells' capability to migrate through the Boyden chambers nearly 2-fold (Figure 7A), whereas overexpression of KDM5B decreased the cell migratory potential by 50% (Figure 7B). To determine the effect of KDM5B on cell invasion potential, MDA-MB-231 cells were tested in Matrigel-coated chambers. The invaded cells were fixed, stained with Crystal Violet, and counted using a light

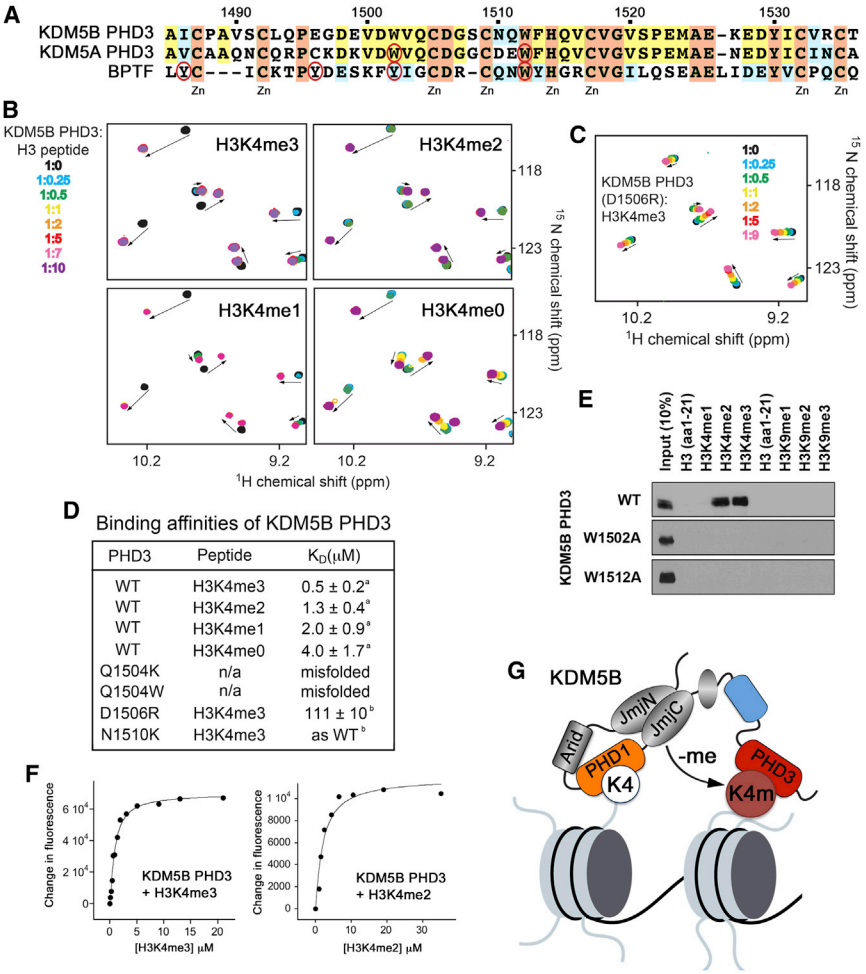

PHD3	Peptide	K_D(μM)
WT	H3K4me3	0.5 ± 0.2[a]
WT	H3K4me2	1.3 ± 0.4[a]
WT	H3K4me1	2.0 ± 0.9[a]
WT	H3K4me0	4.0 ± 1.7[a]
Q1504K	n/a	misfolded
Q1504W	n/a	misfolded
D1506R	H3K4me3	111 ± 10[b]
N1510K	H3K4me3	as WT[b]

Figure 6. The PHD3 Finger of KDM5B Is Selective for H3K4me3

(A) Alignment of the PHD finger sequences; absolutely, moderately, and weakly conserved residues are colored pink, yellow, and blue, respectively. The Lys4me3 binding residues are indicated by red ovals. Each tenth residue of KDM5B is labeled.

(B and C) Superimposed $^{1}H,^{15}N$ HSQC spectra of KDM5B PHD3, WT, or D1506R collected upon titration with the indicated peptides.

(D) Binding affinities of the KDM5B PHD3 finger as measured by tryptophan fluorescence ([a]) or NMR ([b]).

(E) Western blot analysis of GST-KDM5B PHD3, WT, and mutants bound to the indicated biotinylated peptides.

(F) Representative binding curves used to determine K_D values by fluorescence.

(G) Model for KDM5B anchoring at chromatin and spreading the transcriptionally inactive state.

See also Figure S4.

231 cancer cells, whereas recognition of H3K4me3 by the PHD3 finger of KDM5B is dispensable in suppression of cell migration.

Conclusions

Previous observations and data presented in this study demonstrate that the expression level of KDM5B is highly cancer cell-type dependent. KDM5B is downregulated in ER^{-} breast cancer cells, including MDA-MB 231 triple-negative breast cancer cells, whereas, in line with previous findings (Hayami et al., 2010; Scibetta et al., 2007; Yamane et al., 2007), it is upregulated in ER^{+} breast cancer cells, such as MCF7. Depending on the type of cancer cells, KDM5B appears to elicit opposite effects, acting much like other major transcriptional regulators p53 and TGF-β: in contrast to its tumor-promoting function in MCF7 cells (Catchpole et al., 2011; Li et al., 2011; Yamane et al., 2007), KDM5B inhibits the migration and invasion of MDA-MB 231 cells.

Our structural and biochemical analyses reveal that two of the PHD fingers of KDM5B, PHD1 and PHD3, associate with histone tails. The PHD1 finger specifically binds to H3K4me0, and the PHD3 finger is selective for H3K4me3. Thus, not only does the KDM5B demethylase erase the H3K4me3/2/1 marks, producing unmodified H3K4me0, it also reads the target mark and the product of its own catalytic activity through distinct PHD fingers. The combination of two "readers" capable of recognizing distinctive epigenetic marks is likely to have a significant impact on KDM5B activity. Binding of PHD1 to H3K4me0 may provide an anchoring mechanism for KDM5B to sense H3K4me3 through PHD3 and slide along the H3K4me3-enriched promoters, demethylating nearby methylated H3K4 and further spreading the transcriptionally inactive state of chromatin (Figure 6G). Furthermore, the ability of the PHD3 finger to bind unmodified H3 as well

microscope (Figure 7C). We found that overexpression of KDM5B reduced the MDA-MB-231 cell invasion potential. Thus, KDM5B is required to block the migration and invasion ability of ER^{-}-type triple-negative breast cancer cells.

To determine the role of the PHD fingers and their histone binding in MDA-MB 231 cell migration, we generated cell lines stably expressing full-length wild-type (WT) KDM5B and KDM5B mutants harboring loss-of-function mutations either in the PHD1 finger (L326W and D328A) or in the PHD3 finger (W1502A) (Figure 7D, right). These stable cell lines were then used in cell migration assays. As expected, WT KDM5B decreased cell migration by 50% compared with the control cells; however, the L326W and D328A mutants of PHD1 that were impaired in binding to H3K4me0 failed to suppress cell migration (Figure 7D, left). These results suggest that the PHD1 finger mutants may act as dominant-negative mutants, altering the dynamics and interactions of endogenous KDM5B. In contrast, the W1502A mutant of PHD3 that was defective in H3K4me3 binding showed an inhibitory effect on cell migration similar to the effect of the WT protein. These results suggest that recognition of H3K4me0 by the PHD1 finger of KDM5B is important for inhibiting migration of MDA-MB

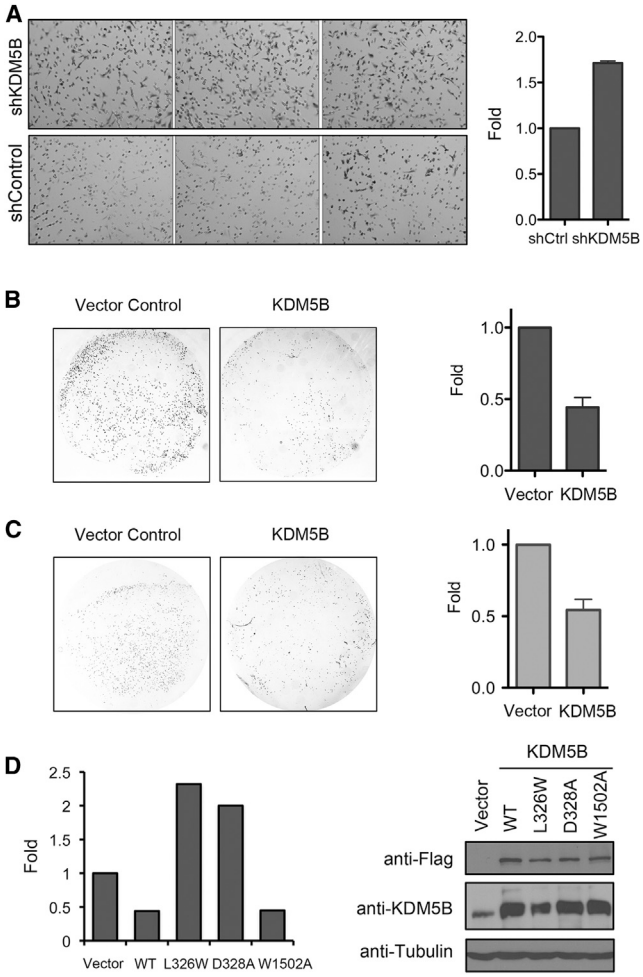

Figure 7. KDM5B Represses Cell Migration in a PHD1-Dependent Manner

(A) Knockdown of KDM5B increases cell migration. Representative views of cells that migrated through the Boyden chambers. An averaged migration activity of KDM5B knockdown cells (relative to control cells) from three independent experiments is shown on the right.

(B and C) Overexpression of KDM5B represses cell migration and invasion activities of MDA-MB 231 cells. Representative views of cells that migrated through the Boyden chambers (B) or extracellular matrix-coated chambers (C) are shown. Averaged migration (B) and invasion activity (C) of KDM5B-expressing cells (relative to control cells) from three independent experiments are shown on the right. Error bars represent SEM.

(D) Repression of cell migration by KDM5B requires histone binding of PHD1, but not histone binding of PHD3. Shown are averaged cell migration activities of MDA-MB 231 cells expressing WT or mutated PHD1 and PHD3 (left), and expression levels of the KDM5B proteins (right).

implies that the sliding process may also occur when the H3K4me3 level is low.

The finding that KDM5B is copurified and colocalizes with components of the NuRD complex indicates that KDM5B and NuRD may cooperate in transcriptional repression (Figure 2C). The NuRD complex contains two catalytic subunits, the deacetylase HDAC1 and the CHD4 ATPase, both of which are essential for the regulation of gene expression and chromatin remodeling. The cooperative action of the three catalytic proteins—KDM5B, HDAC1, and CHD4—links H3K4 demethylation, lysine deacetylation, and ATPase-mediated chromatin remodeling and can provide a powerful mechanism for a rapid shutoff of actively transcribed genes (Figure 2C). Multiple contacts of other NuRD components with chromatin likely add another layer of complexity. Histone-binding activities of two PHD fingers of CHD4 and the WD40 domain of RBBP7/4, as well as DNA binding by the ARID domain of KDM5B and two chromodomains of CHD4 may fine-tune the affinity and specificity of this gene repressive machinery (Bouazoune et al., 2002; Murzina et al., 2008; Musselman et al., 2009; Scibetta et al., 2007). Future functional studies are necessary to establish the importance of crosstalk between these epigenetic components in KDM5B-mediated transcriptional repression.

EXPERIMENTAL PROCEDURES

NMR Spectroscopy and Sequence-Specific Resonance Assignments

NMR experiments were performed at 298K on a Varian INOVA 600 MHz spectrometer equipped with a cryogenic probe. For backbone assignments, uniformly ^{15}N- and ^{13}C-labeled KDM5B PHD1 (1 mM in Tris-HCl buffer pH 6.8, 150 mM NaCl, 15 mM dithiothreitol, and 8% D_2O) was used to perform 3D triple-resonance HNCACB, CBCA(CO)NH, C(CO)NH, and HC(CO)NH experiments as described previously (Ali et al., 2013). The NMR data were processed with nmrPipe (Delaglio et al., 1995) and analyzed with nmrDraw. Initial sequence-specific assignments were obtained in the PINE program and completed using CcpNMR Analysis v1.6 (Vranken et al., 2005).

Chemical-shift perturbation experiments were carried out using 0.1 mM uniformly ^{15}N-labeled WT or mutated KDM5B PHD1, KDM5B PHD3, KDM5D PHD1, and yeast KDM5 PHD fingers. The ^{1}H,^{15}N HSQC spectra were recorded in the presence of increasing concentrations of 12-mer histone tail peptides (synthesized by the University of Colorado Denver Peptide Core Facility). The K_D values were determined by a nonlinear least-squares analysis in Kaleidagraph using the following equation:

$$\Delta\delta = \Delta\delta_{max}\left(([L]+[P]+K_d) - \sqrt{([L]+[P]+K_d)^2 - 4[P][L]}\right)\Big/2[P]$$

where [*L*] is concentration of the peptide, [*P*] is the concentration of the protein, $\Delta\delta$ is the observed chemical shift change, and $\Delta\delta_{max}$ is the normalized chemical-shift change at saturation. Normalized (Grzesiek et al., 1996) chemical-shift changes were calculated using the equation $\Delta\delta = \sqrt{(\Delta\delta H)^2 + (\Delta\delta N/5)^2}$, where $\Delta\delta$ is the change in chemical shift in parts per million (ppm).

Fluorescence Spectroscopy

Spectra were recorded at 25°C on a Fluoromax-3 spectrofluorometer (HORIBA). Samples containing KDM5B PHD1 and PHD3 fingers in PBS buffer and progressively increasing concentrations of the histone peptide were excited at 295 nm or 280 nm. Emission spectra were recorded over a range of wavelengths between 305 and 405 nm with a 0.5 nm step size and a 1 s integration time. Three scans were averaged and recorded. K_D values were calculated using a nonlinear least-squares analysis and the following equation:

$$\Delta I = \Delta I_{max}\left(([L]+[P]+K_d) - \sqrt{([L]+[P]+K_d)^2 - 4[P][L]}\right)\Big/2[P]$$

where [*L*] is the concentration of the histone peptide, [*P*] is the concentration of KDM5B PHD1 or KDM5B PHD3, ΔI is the observed change of signal intensity, and ΔI_{max} is the difference in signal intensity of the free and bound states of the PHD finger. K_D represents the average of three separate experiments (two for the PHD1-H3K4me2 interaction), with error computed as the SD between those values.

Cell Migration and Invasion Assays

Cell migration and invasion assays were performed as described previously using Boyden chambers (BD Biosciences) and modified Boyden chambers coated with Matrigel matrix (Li et al., 2011). MDA-MB 231 cells (1×10^5) were starved for 16–20 hr in Dulbecco's modified Eagle's medium containing 0.1% BSA, and then in 300 μl serum-free medium, and were placed in the upper chamber of the transwell. The chambers were then transferred to 24-well plates containing 500 μl of media supplemented with 10% fetal bovine serum in each well and were incubated for less than 24 hr at 37°C. Noninvading cells were removed by wiping the upper side of the membrane, and the invaded cells were fixed and stained with Crystal Violet. The number of invaded cells was counted under a light microscope from at least five fields and three experiments. The average numbers from the three experiments were calculated between control and the samples using Student's t test.

SUPPLEMENTAL INFORMATION

Supplemental Information includes Supplemental Experimental Procedures, four figures, and four tables and can be found with this article online at http://dx.doi.org/10.1016/j.celrep.2013.12.021.

ACKNOWLEDGMENTS

This work was supported by grants from the NIH (GM096863 and GM101664 to T.G.K., R01HG007538 to W.L., HL65440 to M.G., GM068088 to B.D.S., and GM063873 to D.L.B.), CPRIT (RP110471 to X.S. and W.L.), the Welch Foundation (G1719 to X.S.), and the American Cancer Society (RSG-13-290-01-TBE to X.S.). W.L. is a recipient of a Duncan Scholar Award, and X.S. is a recipient of a Kimmel Scholar Award. S.B.R. is a postdoctoral fellow of the American Cancer Society (PF-13-085-01-DMC). B.J.K. was supported by NIH Postdoctoral Training Grant T32AA007464 and is an American Heart Association postdoctoral fellow.

Received: August 3, 2013
Revised: October 24, 2013
Accepted: December 12, 2013
Published: January 9, 2014

REFERENCES

Ali, M., Rincón-Arano, H., Zhao, W., Rothbart, S.B., Tong, Q., Parkhurst, S.M., Strahl, B.D., Deng, L.W., Groudine, M., and Kutateladze, T.G. (2013). Molecular basis for chromatin binding and regulation of MLL5. Proc. Natl. Acad. Sci. USA *110*, 11296–11301.

Allen, H.F., Wade, P.A., and Kutateladze, T.G. (2013). The NuRD architecture. Cell. Mol. Life Sci. *70*, 3513–3524.

Barrett, A., Santangelo, S., Tan, K., Catchpole, S., Roberts, K., Spencer-Dene, B., Hall, D., Scibetta, A., Burchell, J., Verdin, E., et al. (2007). Breast cancer associated transcriptional repressor PLU-1/JARID1B interacts directly with histone deacetylases. Int. J. Cancer *121*, 265–275.

Bouazoune, K., Mitterweger, A., Längst, G., Imhof, A., Akhtar, A., Becker, P.B., and Brehm, A. (2002). The dMi-2 chromodomains are DNA binding modules important for ATP-dependent nucleosome mobilization. EMBO J. *21*, 2430–2440.

Catchpole, S., Spencer-Dene, B., Hall, D., Santangelo, S., Rosewell, I., Guenatri, M., Beatson, R., Scibetta, A.G., Burchell, J.M., and Taylor-Papadimitriou, J. (2011). PLU-1/JARID1B/KDM5B is required for embryonic survival and contributes to cell proliferation in the mammary gland and in ER+ breast cancer cells. Int. J. Oncol. *38*, 1267–1277.

Chicas, A., Kapoor, A., Wang, X., Aksoy, O., Evertts, A.G., Zhang, M.Q., Garcia, B.A., Bernstein, E., and Lowe, S.W. (2012). H3K4 demethylation by Jarid1a and Jarid1b contributes to retinoblastoma-mediated gene silencing during cellular senescence. Proc. Natl. Acad. Sci. USA *109*, 8971–8976.

Christensen, J., Agger, K., Cloos, P.A., Pasini, D., Rose, S., Sennels, L., Rappsilber, J., Hansen, K.H., Salcini, A.E., and Helin, K. (2007). RBP2 belongs to a family of demethylases, specific for tri-and dimethylated lysine 4 on histone 3. Cell *128*, 1063–1076.

Cloos, P.A., Christensen, J., Agger, K., and Helin, K. (2008). Erasing the methyl mark: histone demethylases at the center of cellular differentiation and disease. Genes Dev. *22*, 1115–1140.

Delaglio, F., Grzesiek, S., Vuister, G.W., Zhu, G., Pfeifer, J., and Bax, A. (1995). NMRPipe: a multidimensional spectral processing system based on UNIX pipes. J. Biomol. NMR *6*, 277–293.

Eissenberg, J.C., Lee, M.G., Schneider, J., Ilvarsonn, A., Shiekhattar, R., and Shilatifard, A. (2007). The trithorax-group gene in Drosophila little imaginal discs encodes a trimethylated histone H3 Lys4 demethylase. Nat. Struct. Mol. Biol. *14*, 344–346.

Grzesiek, S., Stahl, S.J., Wingfield, P.T., and Bax, A. (1996). The CD4 determinant for downregulation by HIV-1 Nef directly binds to Nef. Mapping of the Nef binding surface by NMR. Biochemistry *35*, 10256–10261.

Hayami, S., Yoshimatsu, M., Veerakumarasivam, A., Unoki, M., Iwai, Y., Tsunoda, T., Field, H.I., Kelly, J.D., Neal, D.E., Yamaue, H., et al. (2010). Overexpression of the JmjC histone demethylase KDM5B in human carcinogenesis: involvement in the proliferation of cancer cells through the E2F/RB pathway. Mol. Cancer *9*, 59.

Iwase, S., Lan, F., Bayliss, P., de la Torre-Ubieta, L., Huarte, M., Qi, H.H., Whetstine, J.R., Bonni, A., Roberts, T.M., and Shi, Y. (2007). The X-linked mental retardation gene SMCX/JARID1C defines a family of histone H3 lysine 4 demethylases. Cell *128*, 1077–1088.

Klose, R.J., Kallin, E.M., and Zhang, Y. (2006). JmjC-domain-containing proteins and histone demethylation. Nat. Rev. Genet. *7*, 715–727.

Klose, R.J., Yan, Q., Tothova, Z., Yamane, K., Erdjument-Bromage, H., Tempst, P., Gilliland, D.G., Zhang, Y., and Kaelin, W.G., Jr. (2007). The retinoblastoma binding protein RBP2 is an H3K4 demethylase. Cell *128*, 889–900.

Krishnakumar, R., and Kraus, W.L. (2010). PARP-1 regulates chromatin structure and transcription through a KDM5B-dependent pathway. Mol. Cell *39*, 736–749.

Lan, F., Collins, R.E., De Cegli, R., Alpatov, R., Horton, J.R., Shi, X., Gozani, O., Cheng, X., and Shi, Y. (2007). Recognition of unmethylated histone H3 lysine 4 links BHC80 to LSD1-mediated gene repression. Nature *448*, 718–722.

Lee, N., Zhang, J., Klose, R.J., Erdjument-Bromage, H., Tempst, P., Jones, R.S., and Zhang, Y. (2007). The trithorax-group protein Lid is a histone H3 trimethyl-Lys4 demethylase. Nat. Struct. Mol. Biol. *14*, 341–343.

Li, Q., Shi, L., Gui, B., Yu, W., Wang, J., Zhang, D., Han, X., Yao, Z., and Shang, Y. (2011). Binding of the JmjC demethylase JARID1B to LSD1/NuRD suppresses angiogenesis and metastasis in breast cancer cells by repressing chemokine CCL14. Cancer Res. *71*, 6899–6908.

Liang, G., Klose, R.J., Gardner, K.E., and Zhang, Y. (2007). Yeast Jhd2p is a histone H3 Lys4 trimethyl demethylase. Nat. Struct. Mol. Biol. *14*, 243–245.

Morris, S.R., and Carey, L.A. (2007). Molecular profiling in breast cancer. Rev. Endocr. Metab. Disord. *8*, 185–198.

Murzina, N.V., Pei, X.Y., Zhang, W., Sparkes, M., Vicente-Garcia, J., Pratap, J.V., McLaughlin, S.H., Ben-Shahar, T.R., Verreault, A., Luisi, B.F., and Laue, E.D. (2008). Structural basis for the recognition of histone H4 by the histone-chaperone RbAp46. Structure *16*, 1077–1085.

Musselman, C.A., and Kutateladze, T.G. (2011). Handpicking epigenetic marks with PHD fingers. Nucleic Acids Res. *39*, 9061–9071.

Musselman, C.A., Mansfield, R.E., Garske, A.L., Davrazou, F., Kwan, A.H., Oliver, S.S., O'Leary, H., Denu, J.M., Mackay, J.P., and Kutateladze, T.G. (2009). Binding of the CHD4 PHD2 finger to histone H3 is modulated by covalent modifications. Biochem. J. *423*, 179–187.

Nijwening, J.H., Geutjes, E.J., Bernards, R., and Beijersbergen, R.L. (2011). The histone demethylase Jarid1b (Kdm5b) is a novel component of the Rb pathway and associates with E2f-target genes in MEFs during senescence. PLoS ONE *6*, e25235.

Roesch, A., Becker, B., Meyer, S., Wild, P., Hafner, C., Landthaler, M., and Vogt, T. (2005). Retinoblastoma-binding protein 2-homolog 1: a retinoblastoma-binding protein downregulated in malignant melanomas. Mod. Pathol. *18*, 1249–1257.

Roesch, A., Fukunaga-Kalabis, M., Schmidt, E.C., Zabierowski, S.E., Brafford, P.A., Vultur, A., Basu, D., Gimotty, P., Vogt, T., and Herlyn, M. (2010). A temporarily distinct subpopulation of slow-cycling melanoma cells is required for continuous tumor growth. Cell *141*, 583–594.

Scibetta, A.G., Santangelo, S., Coleman, J., Hall, D., Chaplin, T., Copier, J., Catchpole, S., Burchell, J., and Taylor-Papadimitriou, J. (2007). Functional analysis of the transcription repressor PLU-1/JARID1B. Mol. Cell. Biol. *27*, 7220–7235.

Secombe, J., Li, L., Carlos, L., and Eisenman, R.N. (2007). The Trithorax group protein Lid is a trimethyl histone H3K4 demethylase required for dMyc-induced cell growth. Genes Dev. *21*, 537–551.

Seward, D.J., Cubberley, G., Kim, S., Schonewald, M., Zhang, L., Tripet, B., and Bentley, D.L. (2007). Demethylation of trimethylated histone H3 Lys4 in vivo by JARID1 JmjC proteins. Nat. Struct. Mol. Biol. *14*, 240–242.

Shen, Y., Lange, O., Delaglio, F., Rossi, P., Aramini, J.M., Liu, G., Eletsky, A., Wu, Y., Singarapu, K.K., Lemak, A., et al. (2008). Consistent blind protein structure generation from NMR chemical shift data. Proc. Natl. Acad. Sci. USA *105*, 4685–4690.

Vicent, G.P., Nacht, A.S., Zaurin, R., Font-Mateu, J., Soronellas, D., Le Dily, F., Reyes, D., and Beato, M. (2013). Unliganded progesterone receptor-mediated targeting of an RNA-containing repressive complex silences a subset of hormone-inducible genes. Genes Dev. *27*, 1179–1197.

Vranken, W.F., Boucher, W., Stevens, T.J., Fogh, R.H., Pajon, A., Llinas, M., Ulrich, E.L., Markley, J.L., Ionides, J., and Laue, E.D. (2005). The CCPN data model for NMR spectroscopy: development of a software pipeline. Proteins *59*, 687–696.

Wang, G.G., Song, J., Wang, Z., Dormann, H.L., Casadio, F., Li, H., Luo, J.L., Patel, D.J., and Allis, C.D. (2009). Haematopoietic malignancies caused by dysregulation of a chromatin-binding PHD finger. Nature *459*, 847–851.

Xiang, Y., Zhu, Z., Han, G., Ye, X., Xu, B., Peng, Z., Ma, Y., Yu, Y., Lin, H., Chen, A.P., and Chen, C.D. (2007). JARID1B is a histone H3 lysine 4 demethylase up-regulated in prostate cancer. Proc. Natl. Acad. Sci. USA *104*, 19226–19231.

Yamane, K., Tateishi, K., Klose, R.J., Fang, J., Fabrizio, L.A., Erdjument-Bromage, H., Taylor-Papadimitriou, J., Tempst, P., and Zhang, Y. (2007). PLU-1 is an H3K4 demethylase involved in transcriptional repression and breast cancer cell proliferation. Mol. Cell *25*, 801–812.

Yoshida, M., Ishimura, A., Terashima, M., Enkhbaatar, Z., Nozaki, N., Satou, K., and Suzuki, T. (2011). PLU1 histone demethylase decreases the expression of KAT5 and enhances the invasive activity of the cells. Biochem. J. *437*, 555–564.